

Assessing the Performance of Different Large Format Digital Cameras by investigating the Geometric Accuracy and Camera Calibration

Khaldoun Qtaishat
Mutah University, Karak, Jordan

Key words: large format digital camera, interior calibration, geometry.

ABSTRACT

This paper provides independent investigations in the geometric accuracy and camera calibration of the new photogrammetric digital airborne cameras systems which was undertaken as a part of the German Society of Photogrammetry, Remote Sensing and Geoinformation (DGPF) project for investigating large format digital cameras (Vexcel Imaging UltraCamX, ZAI Imaging DMC, and ZAI Imaging RMC Top 15). This paper present results form the imaging data which was flown at 6 different flight days flown over a test site in Germany during a 10 weeks time window starting beginning of July till mid of September 2008. Most of the sensors were flown in two different flying heights, resulting in two blocks with different ground sampling distance (GSD), namely GSD 20cm and GSD 8cm.

In this paper, the digital camera calibration was assessed throught analysing and identifying any systematic patterns in the image residuals. A new calibration methos was undertaken in this paper based on analysing the systematic errors of the high and low flown residual. The bundle adjustment will be re-computed based on the analysis of the systematic residual patterns. This approach is based on analysing the systematic errors of the high flown residual and re-computing the bundle adjustment of the low flown images based on the residual corrections of the high flown images. These corrections were computed from a block triangulation and applied because the systematic pattern was considered to be similar to all images.

The bundle adjustment will be re-computed based on the analysis of the systematic residual patterns. This approach is based on analysing the systematic errors of the high flown residual and re-computing the bundle adjustment of the low flown images based on the residual corrections of the high flown images.

The results which introduced in this paper were significantly improved by using the traditional existing self calibration methods and the new calibration approach.

1. INTRODUCTION

In these days, large format digital aerial cameras are increasingly replacing analogue aerial cameras, even in some countries, analogue aerial cameras are no longer accepted (Jacobsen, 2009). It was approximately 8 years ago when first two commercial large format digital airborne cameras; DMC and ADS40, were lunched at the Amsterdam

ISPRS congress. The large format digital aerial cameras are now playing a significant role in the field of digital airborne imaging (Gruber et al., 2006). The geometric model of the sensing system should be determined to any block of images used for a high precision measurement purposes in photogrammetry (Cramer, 2005). In the frame cameras, the relationship of this sensor model to the perspective geometry which used in photogrammetry should be determined. So, the camera calibration which is normally undertaken by the manufacturer before selling the camera can be defined as the processes of measuring the relationship of the perspective geometry and the actual frame camera geometry (Smith et al., 2007).

The new large format digital camera systems are geometrically complex systems because a various groups of CCD arrays are shared to produce a number of images from different perspectives. These images are joining together from multiple lenses to produce a single image which is used for photogrammetry analysis. So, it is required to understand the geometry model of these cameras and analyse the relationship between the perspective geometry and the calibrated camera geometry. The geometric potential of the digital cameras will affect the evaluation of the photogrammetric models (Smith et al., 2005).

This paper provides an investigation into the large format digital camera geometry based on results achieved from two height flights flown over a test site in Germany as part of DGPF project, resulting in two blocks with different ground sampling distance (GSD), namely GSD 20cm and GSD 8cm. The high flight block (GSD=20cm) was flown with forward overlap 60%, while the low flight block (GSD=8cm) was flown with 80% forward overlap. To allow for an inclusive comparison between all the cameras, the test flights were flown in similar conditions.

The quality of large format digital cameras is affected by many factors, ranging from the image measurement quality to the calibration of the integrated systems and the data processing strategies (Kruck, 2006). The strengths and weaknesses of these cameras can be measured by several parameters. One way of assessing this performance is by comparing the digital camera to the traditional film based camera (Cramer et al., 2009). The photogrammetric and photographic issues should be taken in the account when this comparison is performed. In order to investigate the quality of the large format digital cameras performance (DMC and UltraCamX) in this paper, the geometric performance of these cameras was compared to geometric performance from RMK TOP 15 camera.

2. AIM

The aim of this paper was to investigate the geometry strengths and weaknesses of these large format aerial digital cameras. This will involve investigating the following objectives (Smith et al., 2006):

1. Understanding the geometry of these large format aerial digital cameras.
2. Investigate an alternative camera calibration method.
3. Focusing on the analysis of geometric accuracy and sensor calibration.

The main aim of this paper is to derive the sensor specific strengths and maybe weaknesses, which are of relevance when later choosing a sensor for specific applications.

3. METHODOLOGY

The DGPF project provided a data set taken at two different altitudes over a targeted (pre-marked) test site in Vaihingen/Geramny. The methods used for the calibration model are as follows:

1. The Aerial triangulation (AT) will be achieved without any calibration model. The results from this scenario will be considered as a benchmark result.
2. The Aerial triangulation (AT) will be performed with the traditional self calibration methods (1-12 additional parameters). These models were used traditionally with the large format film aerial cameras.
3. In this scenario, the systematic patterns in the image residuals should be identified and analysed from the aerial triangulation through the individual sub-images and the whole image. The bundle adjustment will be re-computed based on the analysis of the systematic residual patterns. This approach is based on analysing the systematic errors of the high flown residual and re-computing the bundle adjustment of the low flown images based on the residual corrections of the high flown images. This scenario will be investigated and it will be considered as a new approach. In this scenario, image residuals from all images will be explored in a sub-area of the image and the systematic patterns will be showed by the image residuals which representing the sub-area. This could involve dividing the image into 25x25 sub-areas. Investigating residual plots of various numbers of subdivisions from one residual per CCD up to a high density of points per CCD the 25x25 division seems to give a reasonably detailed distribution of residuals. The 25x25 also appeared to give a reasonable indication of any systematic patterns and therefore image coordinate correction (Smith et al., 2006).

Two softwares were used in this research; Leica LPS which used for image observations and automatic tie point measurements, and the Institute of Photogrammetry and Geoinformation Leibniz University Hannover Program System (BLUH) analysis tools which used to analyse the results.

4. TEST SITE AND DATA PROVIDED

The DGPF project consisting a data set taken at two different altitudes over a targeted (pre-marked) test site in Vaihingen/Geramny. The following block data sets were utilized within the test process, figure 1 to figure 6 show the UltraCamX, the DMC, and the RMK TOP 15 images blocks respectively, taken at ground sample distance (GSD) of 8 cm and 20 cm.

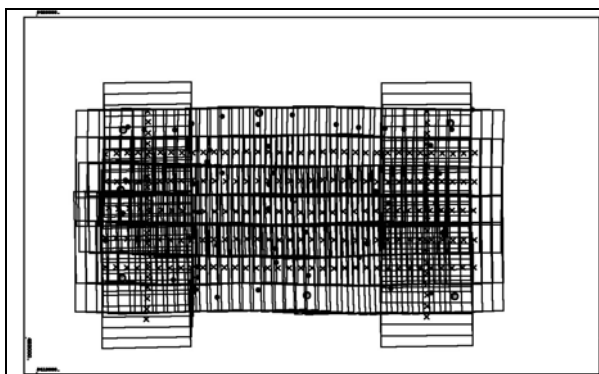


Figure 1: UltraCamX-block with 8cm GSD

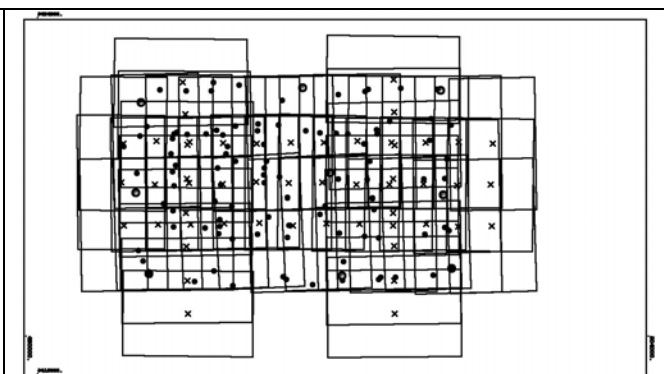


Figure 2: UltraCamX-block with 20cm GSD

The actual pixel size of the object 8cm GSD Blocks UltraCamX is 8.6 cm and the 20cm GSD-block 20.6 cm. The UltraCamX block with 8cm GSD contains 215 images with a longitudinal coverage of 81% and 65% of congruent across, as well as 2 horizontal stripes (Fig. 1). The UltraCamX block with 20cm GSD contains 52 images with a longitudinal coverage of 70% and 70% of congruent across, as well as 2 horizontal stripes (Fig. 2). In the 8cm GSD block, the images contained on average of 250 object points, while in the 20cm-GSD block, the object points were determined and the images in the middle 449 points abstained.

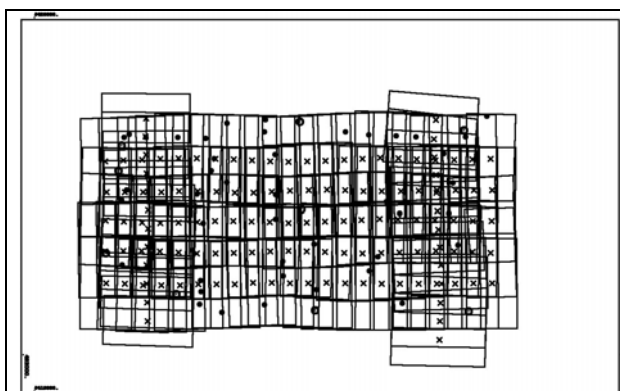


Figure 3: DMC-block with 8cm GSD

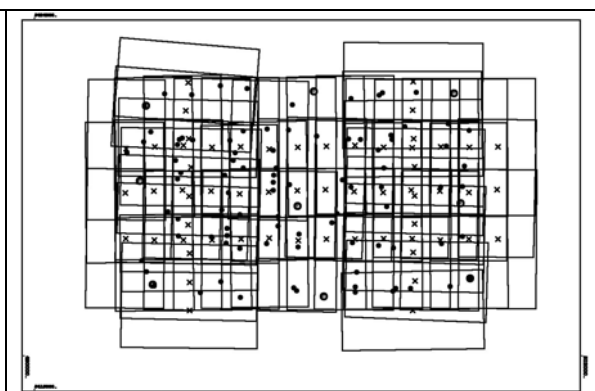


Figure 4: DMC-block with 20cm GSD

The actual pixel size of the object 8cm GSD Blocks DMC is 8.7 cm and the 20cm GSD-block 21.6 cm. The DMC-block with 8cm GSD nominally contains 135 images with longitudinal and congruent across of 60%, and 2 stripes (Fig. 3). The DMC-block with 20cm GSD contains 60 images with longitudinal and congruent across of 60%, and also 2 stripes (Fig. 4). In the 8cm GSD block, the images contained an average of 139 object points, while in the 20cm-GSD block the images contained an average of 177 object points.

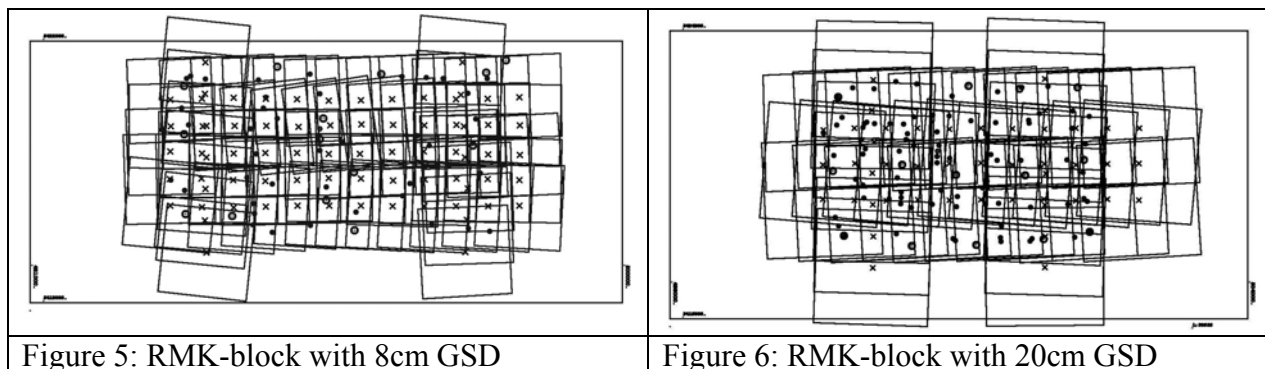


Figure 5: RMK-block with 8cm GSD

Figure 6: RMK-block with 20cm GSD

The RMK-block with 8cm GSD contains 74 images with a longitudinal and congruent across of 60%, and 2 horizontal stripes. 8cm GSD matched to $14\mu\text{m}$ pixel size in the picture (Fig. 5). The RMK-block with 20cm GSD contains 47 images with longitudinal and congruent across of 60%, and 2 stripes (Fig. 6). 20cm GSD corresponded to $14\mu\text{m}$ pixel size in the image. In the 8cm GSD block, the images contain, on average of 125 object points, while in the 20cm-GSD block, the images in the middle 235 points included.

5. RESULTS AND DISCUSSION

5.1 General

It should be noted that the precision of the image observation were relied on the radiometric image quality in both the high and low flight (Smith et al., 2007). The standard error used for the image observations was the σ_0 value from a preliminary run of the aerial triangulation for a particular block being analysed, typically $3\text{-}5\mu\text{m}$. The number of control points and check points used was investigated on the benchmark results, making a reasonable assumption that this would be typical of all other triangulations.

5.2 RESULTS AND DISCUSSION - HIGH FLIGHT (GSD 20CM)

5.2.1 No calibration model - benchmark result

As a camera calibration has already been performed by the vendors, the results were performed in the aerial triangulation without a calibration model which can be used as a 'benchmark result' against which other results can be compared. The results are represented in table 1.

Camera Name/GCP/CP	Ground control points RMSE (m) of residuals			Ground check points RMSE (m) of residuals			Image coordinates RMSE (μm) of residuals		σ_0 μm
	X	Y	Z	X	Y	Z	x	y	
Vexcel Imaging UltraCamX/9/99	0.052	0.061	0.146	0.075	0.083	0.163	0.79	0.85	1.00
Z/I Imaging DMC/9/95	0.031	0.040	0.178	0.045	0.078	0.184	1.45	1.28	1.90
Z/I Imaging RMK Top 15 film/14/82	0.093	0.061	0.130	0.112	0.116	0.154	4.75	4.29	5.90

Table 1. Results of high flight AT without any calibration model
 The following figures indicate the image residuals of the observations in the image space for the results presented in table 1.

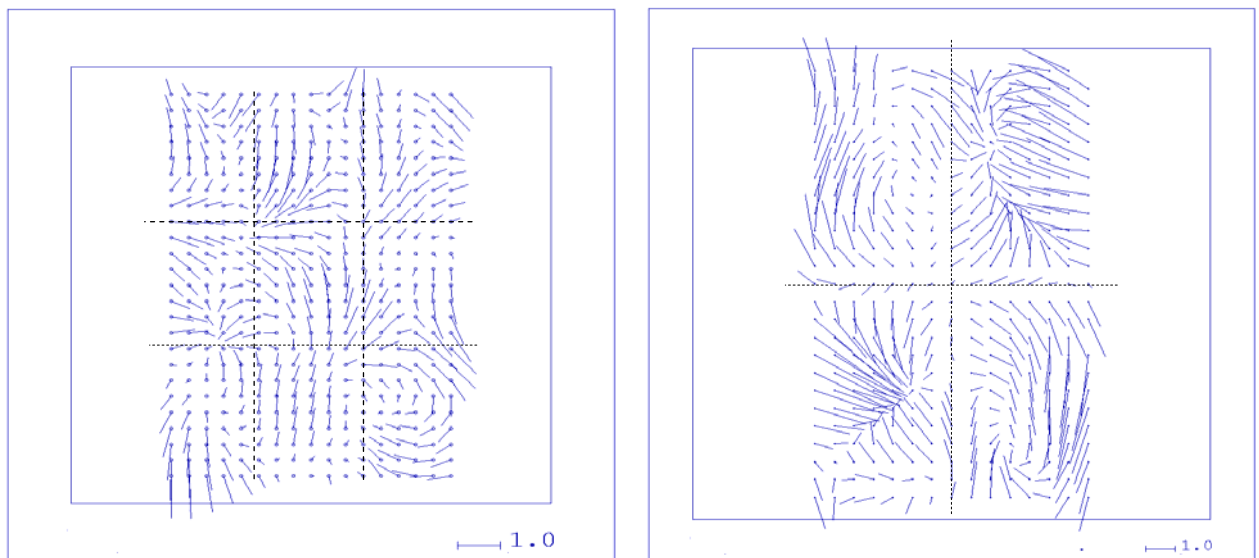


Figure 7. Mean image residuals in 25x25 sub-areas,(UCX on the left and DMC on the right) results of AT without any calibration model (coordinates in μm , partitioning shows approximate boundaries of the CCD arrays)

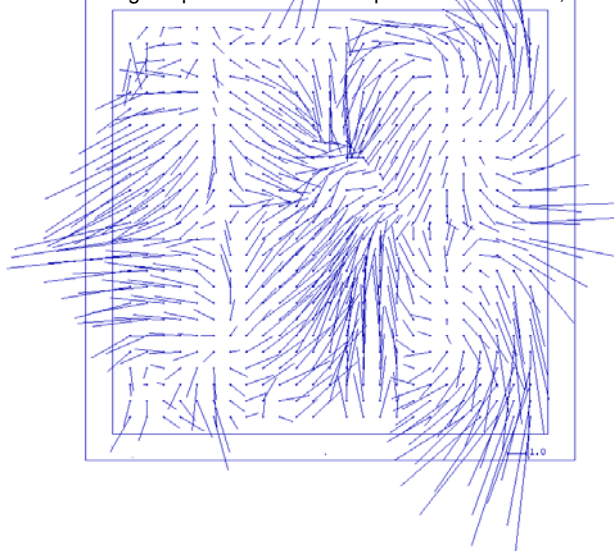


Figure 8. Mean image residuals in 25x25 sub-areas,(Z/I Imaging RMK Top 15 film camera) results of AT without any calibration model (coordinates in μm , partitioning shows approximate boundaries of the CCD arrays)

On visual inspection of figure 7 and figure 8, there are overall identifiable systematic patterns in the whole image for all the three cameras, especially in figure 8 for the film camera RMK Top 15. In figure 7, there are small areas where systematic patterns can be identified, especially with DMC camera, some showing a relationship to the CCDs (9 CCDs for UltraCamX and 4 CCDs for DMC). As these residuals could come from a variety of sources and this is only results from one block, these patterns may not be due to uncorrected systematic characteristics of camera/image geometry.

5.2.2 The result from existing self-calibration models

A number of self calibration models were tested to assess the most suitable for this type of imagery. The results presented here come from the traditional additional parameters in the BLUH software, and are considered as the best result from existing self-calibration models based on the smallest image residuals and RMSE of ground and check points. The parameters of the self-calibration model are as follows (Smith et al., 2006):

c = principal distance

x_0, y_0 = principal point position

a_1, a_2, a_3 = polynomial coefficients for radial lens distortions

The results in table 2 show a very significant improvement in Z coordinates compared to the benchmark values in table 1 in the rule for the two cameras (UltraCamX and DMC) by adding the additional parameters of the self calibration model. These additional parameters collect temperature influences on the board of the constants part panchromatic cameras and radial distortion which is part of the cameras. So, a self calibration with additional parameters is needed and particularly improved the height accuracy.

Camera Name/GCP/CP	Ground control points RMSE (m) of residuals			Ground check points RMSE (m) of residuals			Image coordinates RMSE (μm) of residuals		σ_0 μm
	X	Y	Z	X	Y	Z	x	y	
Vexcel Imaging UltraCamX/9/99	0.054	0.059	0.033	0.075	0.082	0.074	0.78	0.82	1.00
Z/I Imaging DMC/9/95	0.029	0.029	0.031	0.042	0.056	0.071	1.32	1.14	1.60
Z/I Imaging RMK Top 15 film/14/82	0.114	0.125	0.080	0.114	0.125	0.080	4.86	4.49	5.20

Table 2. Results of high flight AT with the traditional additional parameters self calibration model

The following figures 9 & 10 show an improvement on the pattern of the image residuals comparing to the bench mark results t in figure 7 and figure 8.

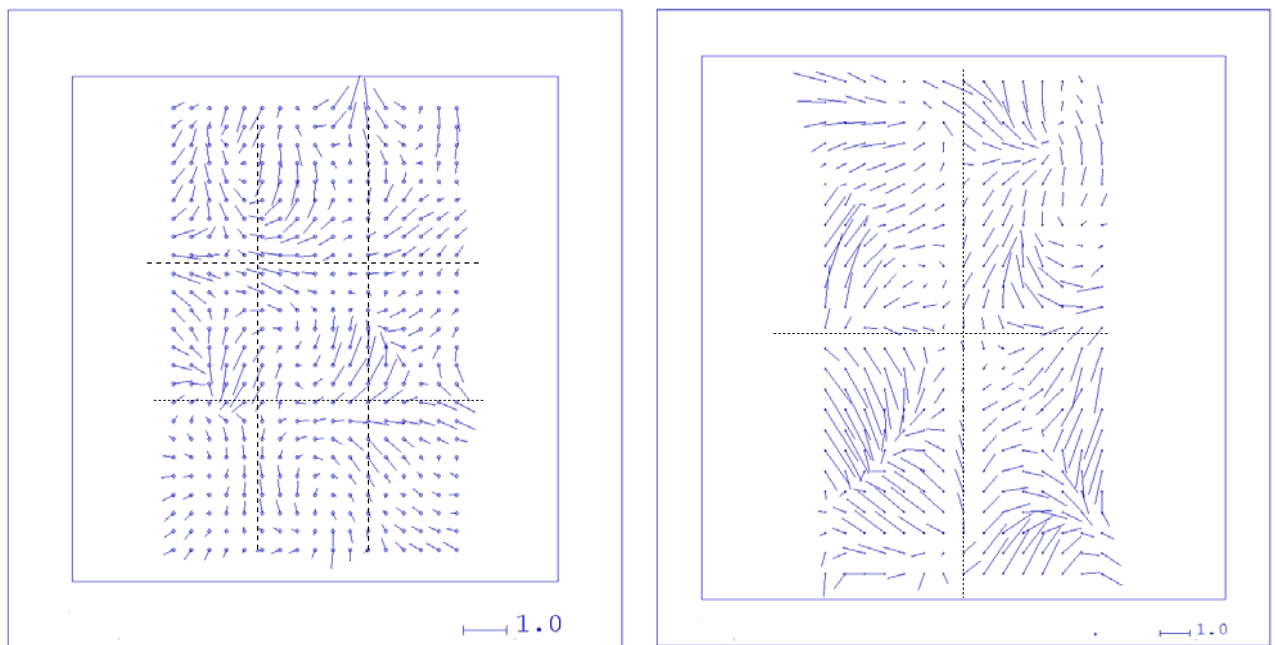


Figure 9. Mean image residuals in 25x25 sub-areas, (UCX on the left and DMC on the right), results of AT with self-calibration model (coordinates in μm , partitioning shows approximate boundaries of the CCD arrays)

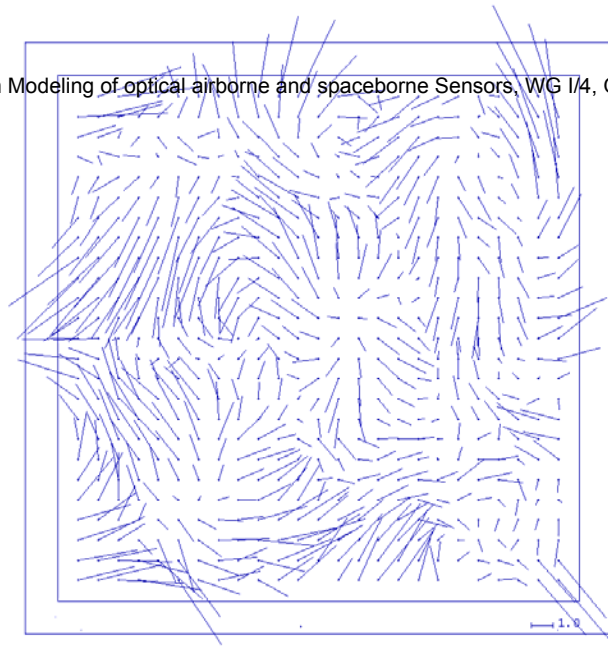


Figure 10. Mean image residuals in 25x25 sub-areas,(Z/I Imaging RMK Top 15) results of AT with self-calibration model (coordinates in μm , partitioning shows approximate boundaries of the CCD arrays)

5.2.3 Analysis of aerial triangulation image residuals

As the geometry of the large format digital cameras is different from the traditional single cone/CCD camera an analysis will be undertaken to try to identify any systematic patterns in the image residuals. This will enable alternative calibration procedures to be considered. The potential camera features which may cause variations from the traditional self-calibration models will be investigating through analysis of triangulation image residuals.

Applying the results shown in figure 7 and figure 8 to the measured image coordinates, as described in the methodology (Approach 3), give the results in table 3 using BLUH software without any self-calibrating model.

Camera Name/GCP/CP	Ground control points RMSE (m) of residuals			Ground check points RMSE (m) of residuals			Image coordinates RMSE (μm) of residuals		σ μm
	X	Y	Z	X	Y	Z	x	y	
Vexcel Imaging UltraCamX/9/99	0.053	0.058	0.125	0.074	0.082	0.143	0.76	0.79	0.90
Z/I Imaging DMC/9/95	0.036	0.032	0.129	0.043	0.066	0.149	1.40	1.19	1.70
Z/I Imaging RMK Top 15 film/14/82	0.093	0.066	0.099	0.114	0.118	0.125	4.57	4.06	5.30

Table 3. Results of high flight AT with analysing the residuals in the aerial triangulation

Applying the results shown in figure 8 and figure 9 to the measured image coordinates by identification and quantification of systematic residuals followed by application to image coordinates and re-computation of the bundle adjustment, as described in the methodology, give the results in table 3, figure 11, and figure 12 using BLUH software without any self-calibrating model. The following figures 11 & 12 show the mean image residuals of the observations for the sub- areas in the image. These figures indicate the image residuals for the results presented in table 3. It appears, from visual inspection, that some of the systematic error patterns have been reduced. As the residuals of UCX camera are so small in figure 11 (left figure) comparing to figure 7 (left figure), the solution appears to have reduced some of the residual pattern although, the residuals in the DMC camera seems to still have some relatively large residuals.

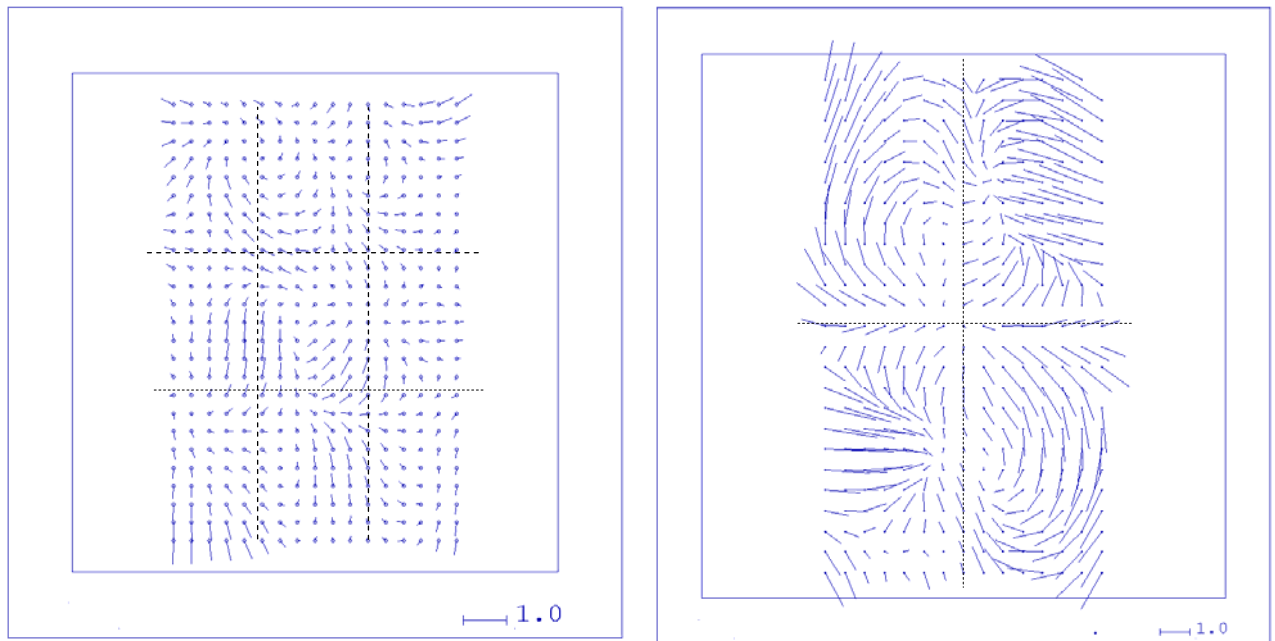


Figure 11. Mean image residuals in 25x25 sub-areas (UCX on the left and DMC on the right), results of AT with adding the residuals approach (coordinates in μm , partitioning shows approximate boundaries of the CCD arrays)

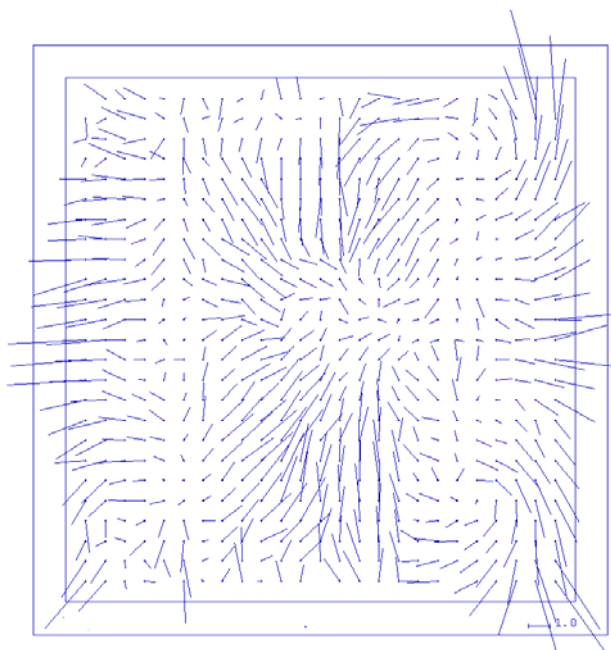


Figure 12. Mean image residuals in 25x25 sub-areas ,(Z/I Imaging RMK Top 15), results of AT with adding the residuals approach (coordinates in μm , partitioning shows approximate boundaries of the CCD arrays)

5.2.4 Summary of high flight results

Table 4 shows the results of the ground control RMSE are significantly better than the ground control check point RMSE values. The ground control RMSE values are influenced by the standard errors of the image coordinates and the ground control. The standard error of $\pm 0.05\text{m}$ for the ground control was provided and the standard error used for the image observations was the σ_0 value from a preliminary run of the aerial triangulation for a particular block being analysed, typically $3\text{-}5\mu\text{m}$. Table 4 also shows in general, a significant improvement has been obtained from the self-calibration model in the Z coordinates for the check control points. The self-calibration model is probably correcting for some environmental effects. The adding residuals approach has slightly improved the RMSE of the image residuals, minimal improvement on the ground and check control RMSE.

Camera Name/GCP/CP	Calibration Model	Ground control points RMSE (m) of residuals			Ground check points RMSE (m) of residuals			Image coordinates RMSE (μm) of residuals		σ_0 μm
		X	Y	Z	X	Y	Z	x	y	
Vexcel Imaging UltraCamX/9/99	No	0.052	0.061	0.146	0.075	0.083	0.163	0.79	0.85	1.00
	Self Calibration	0.054	0.059	0.033	0.075	0.082	0.074	0.78	0.82	1.00
	residuals from high flight	0.053	0.058	0.125	0.074	0.082	0.143	0.76	0.79	0.90
Z/I Imaging DMC/9/95	No	0.031	0.040	0.178	0.045	0.078	0.184	1.45	1.28	1.90
	Self Calibration	0.029	0.029	0.031	0.042	0.056	0.071	1.32	1.14	1.60
	residuals from high flight	0.036	0.032	0.129	0.043	0.066	0.149	1.40	1.19	1.70
Z/I Imaging RMK Top 15 film/14/40	No	0.093	0.061	0.130	0.112	0.116	0.154	4.75	4.29	5.90
	Self Calibration	0.114	0.125	0.080	0.114	0.125	0.080	4.86	4.49	5.20
	residuals from high flight	0.093	0.066	0.099	0.114	0.118	0.125	4.57	4.06	5.30

Table 4. Summary of high flight results

5.3 Results and discussion - low flight (GSD 8cm)

A similar process used for analysing the high flown images has been used to assess the low flown images except for adding the residuals approach, the high flown residual corrections have been used in the low flown computation. This correction was used because the ideal scenario would be to compute the residual corrections from a block of triangulation and then assuming this was a systematic pattern for all images, this would be applied until a new correction was computed. It is important to note that the results from the aerial triangulation in BLUH were obtained with using the cross strips in the low flight.

5.3.1 No calibration model - benchmark result

Camera Name/GCP/CP	Ground control points RMSE (m) of residuals			Ground check points RMSE (m) of residuals			Image coordinates RMSE (μm) of residuals		σ μm
	X	Y	Z	X	Y	Z	x	y	
Vexcel Imaging UltraCamX/9/99	0.029	0.035	0.030	0.044	0.053	0.054	0.75	0.84	0.90
Z/I Imaging DMC/9/95	0.013	0.023	0.044	0.022	0.037	0.077	3.16	2.45	3.30
Z/I Imaging RMK Top 15 film/14/82	0.018	0.031	0.108	0.020	0.040	0.152	4.19	4.17	4.60

Table 5. Results of low flight AT without self-calibration model

It is interesting to note that the image coordinate RMSE values are larger than for the high flight indicating a less quality of measurement and/or image quality. In addition, the difference in the image residuals could have being also influenced by the difference in the number of tie points between the low and high flight. The RMSE values of the ground check points are good in X and Y but the Z value for the check points is a little large compared with the ground control Z value. Figure 13 and figure 14 show the image residuals of the observations in the image space for the results presented in table 5. If there is any systematic pattern in the images then there should be a similarity with the pattern of residuals in figure 7 and figure 8. By visual inspection there is some similarity between the pattern of residuals for UCX camera in figure 7 and figure 13.

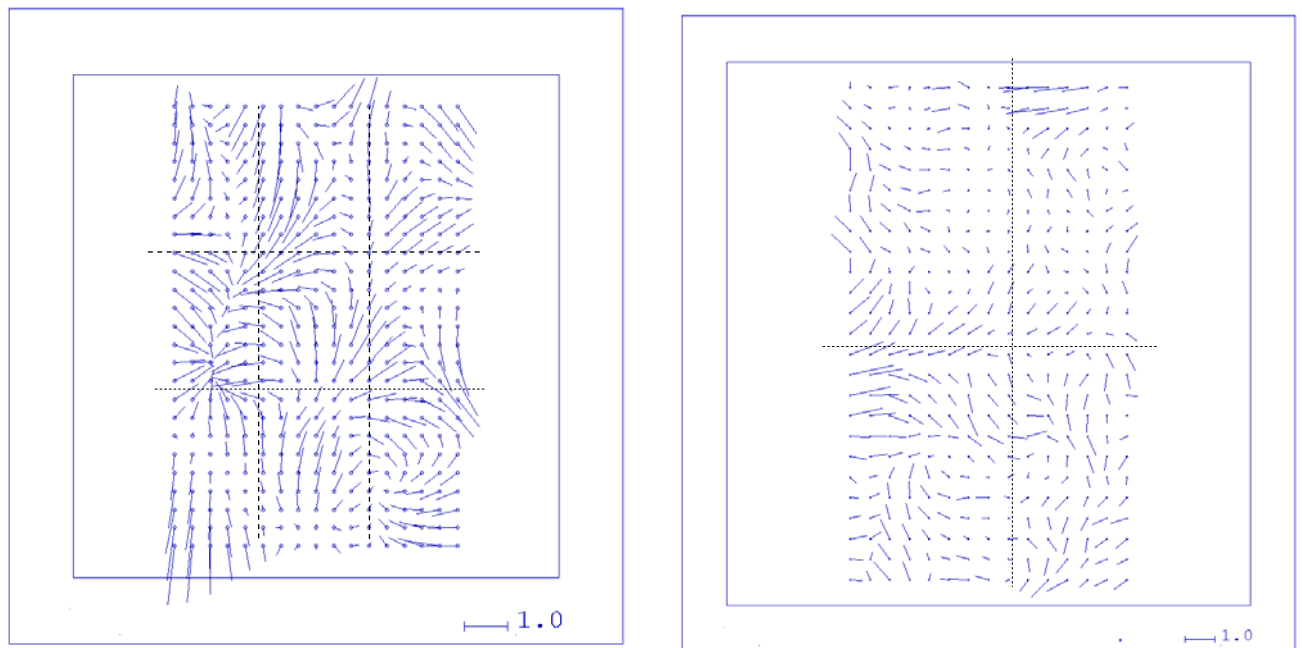


Figure 13. Mean image residuals in 24x24 sub-areas, (UCX on the left and DMC on the right) results of AT without calibration model(coordinates in μm , partitioning shows approximate boundaries of the CCD arrays)

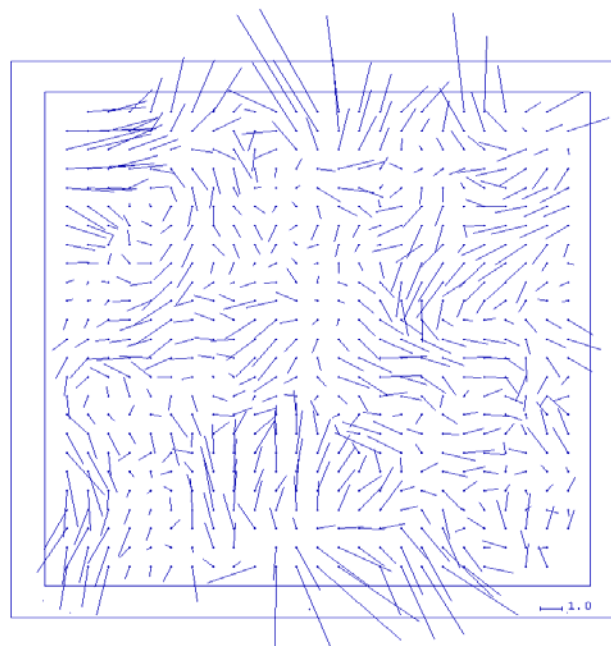


Figure 14. Mean image residuals in 25x25 sub-areas, (Z/I Imaging RMK Top 15) results of AT without calibration model (coordinates in μm , partitioning shows approximate boundaries of the CCD arrays)

5.3.2 The results from existing self-calibration

A number of self-calibration models were tested from BLUH software to assess the most suitable for this type of imagery. The results presented here come from BLUH and are considered the 'best' result from existing self-calibration models based on the smallest image residuals and RMSE of ground and check points. The parameters of the self-calibration model are as follows:

c = principal distance

x_0, y_0 = principal point position

a_1, a_2, a_3 = polynomial coefficients for radial lens distortions

Camera Name/GCP/CP	Ground control points RMSE (m) of residuals			Ground check points RMSE (m) of residuals			Image coordinates RMSE (μm) of residuals		σ μm
	X	Y	Z	X	Y	Z	x	y	
Vexcel Imaging UltraCamX/9/99	0.028	0.033	0.029	0.042	0.050	0.037	0.73	0.80	0.90
Z/I Imaging DMC/9/95	0.014	0.019	0.013	0.023	0.029	0.033	3.07	2.37	3.20
Z/I Imaging RMK Top 15 film/14/82	0.016	0.026	0.038	0.020	0.033	0.049	4.23	4.21	4.30

Table 6. Results of low flight AT with self-calibration model

The following figures indicate the image residuals of the observations in the image space for the results presented in table 6. There is an improvement in the pattern of residuals comparing to those shown in figure 13 and figure 14.

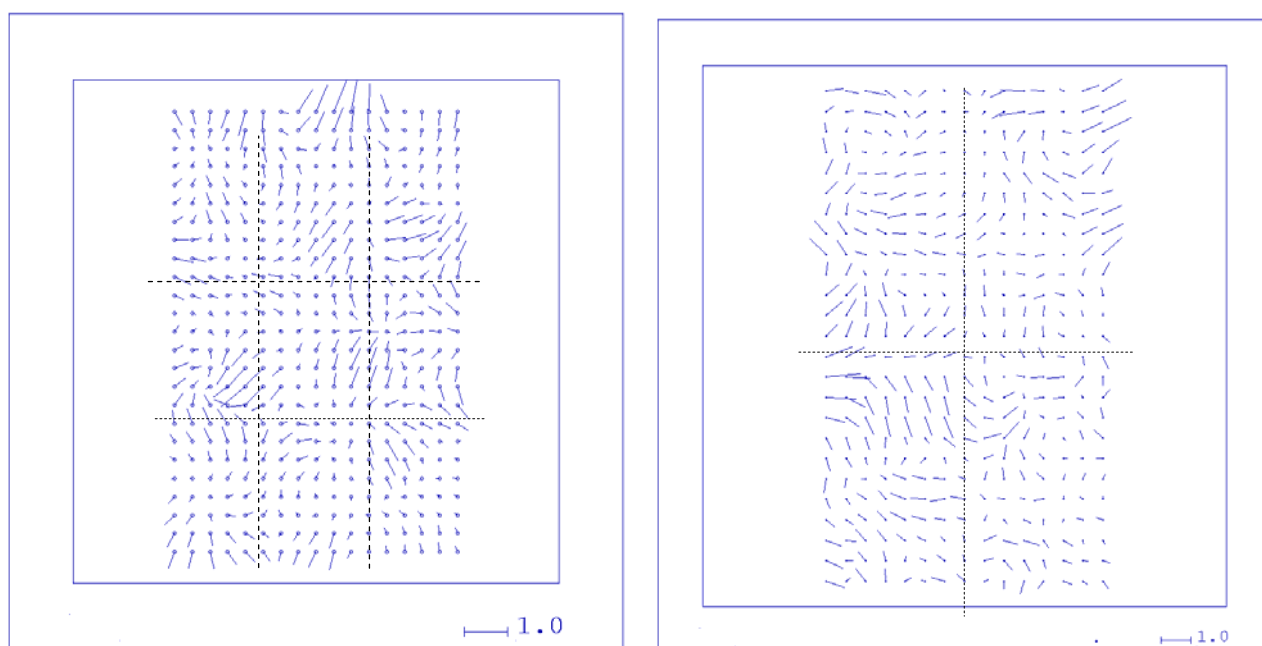


Figure 15. Mean image residuals in 25x25 sub-areas,(UCX on the left and DMC on the right), results of AT with self-calibration model (coordinates in μm , partitioning shows approximate boundaries of the CCD arrays)

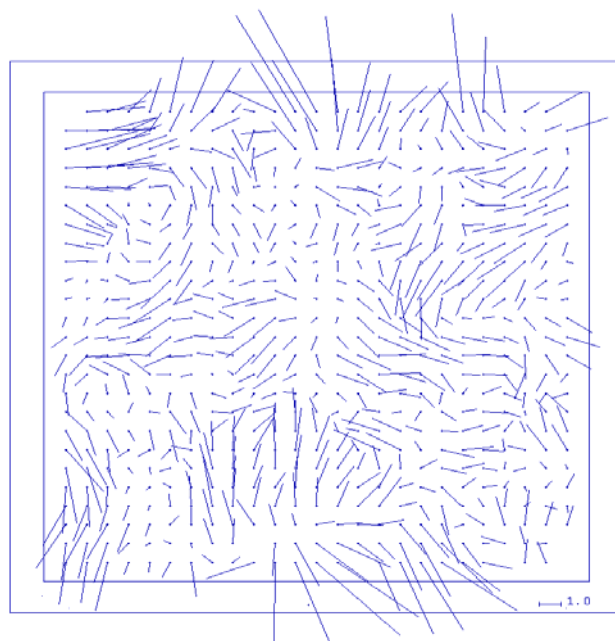


Figure 16. Mean image residuals in 25x25 sub-areas, (Z/I Imaging RMK Top 15) results of AT with self-calibration model (coordinates in μm , partitioning shows approximate boundaries of the CCD arrays)

5.3.3 Analysis of aerial triangulation image residuals from high flight

Camera Name/GCP/CP	Ground control points RMSE (m) of residuals			Ground check points RMSE (m) of residuals			Image coordinates RMSE (μm) of residuals		σ μm
	X	Y	Z	X	Y	Z	x	y	
Vexcel Imaging UltraCamX/9/99	0.028	0.034	0.027	0.044	0.052	0.042	0.72	0.78	0.90
Z/I Imaging DMC/9/95	0.036	0.032	0.129	0.022	0.029	0.041	3.15	2.44	3.20
Z/I Imaging RMK Top 15 film/14/82	0.019	0.029	0.098	0.017	0.030	0.106	4.19	4.17	4.50

Table 7. Results of AT with with analysing the residuals in the aerial triangulation

In this trial, the image coordinate corrections that have been applied are the values computed from the high flown block. The following figures (figure 17 and figure 18) indicate the image residuals of the observations in the image space for the results presented in table 7. It appears, from visual inspection, that some of the patterns have been reduced and there are a significant improvement in the image coordinates comparing to figures 13 & 14.

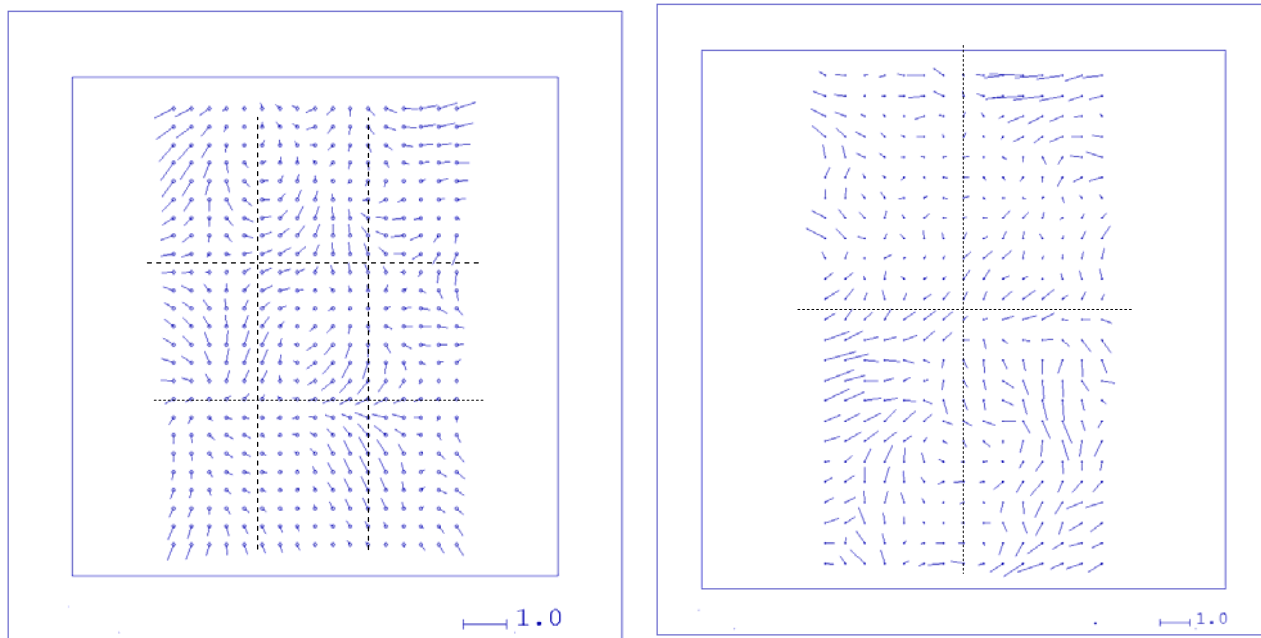


Figure 17. Mean image residuals in 25x25 sub-areas (UCX on the left and DMC on the right), results of AT with adding the high flight residuals (coordinates in μm , partitioning shows approximate boundaries of the CCD arrays)

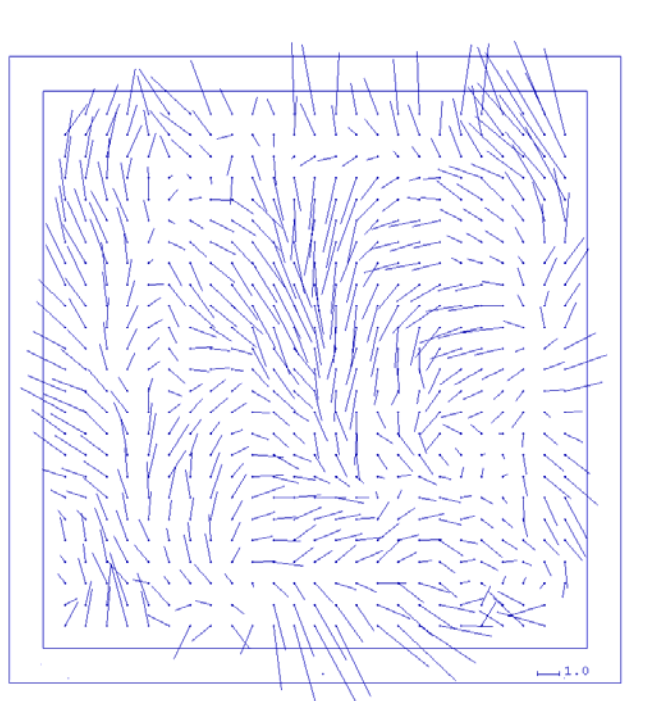


Figure 18. Mean image residuals in 25x25 sub-areas, (Z/I Imaging RMK Top 15), results of AT with adding the residuals approach (coordinates in μm , partitioning shows approximate boundaries of the CCD arrays)

5.3.4 Summary Table 8 of low flight results

Table 8 shows again small RMSE values for the ground control points as identified in the high flown trials. It also shows an improvement in applying a traditional single lens self-calibration model technique, especially in the Z coordinates. The really which has reduced relatively significantly the x and y image residuals and the Z RMSE values for the check points compared to the their bench mark values. This is using the residual corrections from the high flown block.

Camera Name/GCP/CP	Calibration Model	Ground control points RMSE (m) of residuals			Ground check points RMSE (m) of residuals			Image coordinates RMSE (μm) of residuals		σ_0 μm
		X	Y	Z	X	Y	Z	x	y	
Vexcel Imaging UltraCamX/9/99	No	0.029	0.035	0.030	0.044	0.053	0.054	0.75	0.84	0.90
	Self Calibration	0.028	0.033	0.029	0.042	0.050	0.037	0.73	0.80	0.90
	residuals from high flight	0.028	0.034	0.027	0.044	0.052	0.042	0.72	0.78	0.90
Z/I Imaging DMC/9/95	No	0.013	0.023	0.044	0.22	0.037	0.077	3.16	2.45	3.30
	Self Calibration	0.014	0.019	0.013	0.023	0.029	0.033	3.07	2.37	3.20
	residuals from high flight	0.036	0.032	0.129	0.022	0.029	0.041	3.15	2.44	3.20
Z/I Imaging RMK Top 15 film/14/40	No	0.018	0.031	0.108	0.020	0.040	0.152	4.19	4.17	4.60
	Self Calibration	0.016	0.026	0.038	0.020	0.033	0.049	4.23	4.21	4.30
	residuals from high flight	0.019	0.029	0.098	0.017	0.030	0.106	4.19	4.17	4.50

Table 8. Summary of low flight results

6. CONCLUSIONS

Both flights show results where the ground control RMSE is significantly better than the ground control check point RMSE values. This is rather unexpected as we are not conscious of using any incorrect weighing to the control.

Many systematic patterns were visually detected in small areas of the image. The new approach has made a small improvement on the results. This new calibration approach for the low flight has been mostly useful in improving the RMSE in Z and decreasing image residuals. But, the method was less successful at improving the high flown results.

More tests are essential with a number of blocks to fully understand the residual patterns that are being created not only within the images of a block but also among blocks.

The existing self-calibration methods and the adding residuals approach (approach 3) have made a significant improvement on the results. Approach 3 for the low flight has been particularly beneficial in improving the RMSE in Z and reducing image residuals.

However, the method was less successful at improving the high flown results which was used to compute the correction for the low flown blocks.

The new approach has expressed that it needs further investigation to fully assess its capabilities. It is surprising that this new approach did not make as much improvement with the high flown block, which was used to calculate the correction, as it did with the low flown block. Subjects such as optimum subdivision of the image would also need to form part of this study. Similar trials and analyses are being carried out using both the high and the low flown flights altogether.

All investigated systems needed a block triangulation with self calibration by additional parameters or any suitable approach for self calibration. To the cameras adjusted by the new approach described in this paper, the results are improved.

7. REFERENCES

Cramer, M., 2005. Digital Airborne Cameras-Status and Future. ISPRS Hannover Workshop on High resolution Earth imaging for geospatial information Proceedings, Volume XXXVI Part I/W3 ISSN No. 1682-1777.

Cramer, M., Haala, Norbert., 2009. DGPF Project: Evaluation of Digital Photogrammetric Aerial Based Imaging Systems – Overview and Results from the Pilot Centre. ISPRS Hannover Workshop on High resolution Earth imaging for geospatial information Proceedings, Volume XXXVIII-1-4-7_W5.

Gruber M., Ladstädler R., 2006. Geometric Issues of the digital large format aerial camera UltraCamD. International Calibration and Orientation Workshop, EuroCOW 2006. January 2006, Castelldefels, Spain. EuroSDR Commission I and ISPRS Working Group 1/3.

Jacobsen, K., 2009. DGPF-Projekt: Evaluierung digitaler photogrammetrischer Luftbildkamerasysteme – Auswerteteam Geometrie. DGPF Tagungsband 2009

Kruck, E., 2006. Simultaneous Calibration of Digital Aerial Survey Cameras. International Calibration and Orientation Workshop, EuroCOW 2006. January 2006, Castelldefels, Spain. EuroSDR Commission I and ISPRS Working Group 1/3.

SMITH, M. J., KOKKAS, N. AND QTAISHAT, K. S., 2007. Investigation into Self-Calibration methods for the Vexcel UltraCam D Digital Aerial Camera. In: ISPRS Hannover Workshop, High Resolution Earth Imaging for Geospatial Information, 29 May - 1 June. pp. 6

SMITH, M.J., QTAISHAT, K.S., PARK, D.W.G. and JAMIESON, A., 2006. IMU and digital aerial camera misalignment calibration. In: EuroCOW 2006. International Calibration and Orientation Workshop, Castelldefels, Spain, 25-27 January 2006, Castelldefels, Spain.

SMITH, M.J., QTAISHAT, K.S., PARK, D.W.G. and JAMIESON, A., 2005. Initial results from the Vexcel UltraCam digital aerial camera. In: HEIPKE, C., JACOBSON, K., GERKE, M., eds. ISPRS Hannover workshop 2005: High-Resolution Earth Imaging For Geospatial Information, Hannover, Germany. ISPRS, International Society For Photogrammetry and Remote Sensing, v XXXVI, Co I WGI/1, pp. 6